

Supplementary Materials for

Nanometric precision distance metrology via hybrid spectrally-resolved and homodyne interferometry in a single soliton frequency microcomb

Yoon-Soo Jang,^{1,2,*} Hao Liu,^{1,†} Jinghui Yang,¹ Mingbin Yu,³ Dim-Lee Kwong,³ and Chee Wei Wong,^{1*}

¹ Fang Lu Mesoscopic Optics and Quantum Electronics Laboratory, University of California, Los Angeles, CA 90095, USA.

² Length Standards Group, Division of Physical Metrology, Korea Research Institute of Standards and Science (KRISS), 267 Gajeong-ro, Yuseong-gu, Daejeon, 34113, Republic of Korea.

³ Institute of Microelectronics, Singapore 117685, Singapore.

[†] These authors contributed equally to this work.

* ysjang@ucla.edu; cheewei.wong@ucla.edu

This Supplementary Materials consists of the following sections:

Section S1. Data processing for the distance metrology

Section S2. Stable dual-pump generation of the single-soliton frequency microcomb

Section S3. Repetition rate measurement**Section S4. Position calibration of motorized stage by soliton microcomb-based spectrally-resolved interferometry**

Section S5. Gauge block measurement for 3D surface measurement

Section S6. Bounds on the ultimate measurement precision of homodyne interferometry

Section S7. Reference against a stabilized mode-locked fiber laser frequency comb

Section S8. Characterization of intensity fluctuations on the distance metrology

Section S1. Data processing for the distance metrology

S1.A. Fundamental minimum and maximum measurement range

To determine the distance, the reference and measurement pulse should be separated in the time domain. The minimum measurable distance (L_{\min}) is determined by pulse duration used in the distance measurement. L_{\min} can be expressed as $L_{\min} = c_0/(2\Delta\nu)$, where $\Delta\nu$ is a spectrum bandwidth. In our case, L_{\min} is estimated to be 30 μm considering 5 THz spectrum bandwidth of soliton microcomb. The fundamental maximum measurable distance (L_{\max}) is upper-bounded by the coherence length of the light source and can be expressed as $L_{\max} = c_0/(2\delta\nu)$, where $\delta\nu$ is the linewidth of the light source. In our case, the L_{\max} limit is estimated to be 1 km considering the 150 kHz linewidth of soliton microcomb.

S1.B. Nonlinear curve fitting for precise peak detection

To precisely determine the peak position τ_{TOF} in time domain, we implement polynomial curve fitting near peak position as $I(\tau) = A\tau^2 + B\tau + C$. Data points for curve fitting are symmetrically chosen with 3 or 5 points around the peak position. The peak position is determined when its first

derivative is equal to zero as $dI(\tau)/d\tau = 2A\tau + B = 0$. Thus the peak position is simply determined from $\tau = -B/2A$ (detailed in below section).

S1.C. High precision distance measurement by homodyne detection from microcomb spectral interferometry

Spectrally-resolved interferometry [58] has been examined to understand the frequency microcomb coherence [59-62]. Multi-wavelength interference has also been examined for absolute distance metrology [63,64]. For our distance metrology based on the microcomb-enabled spectral resolved interferometry, Figure S1 shows further details on our data processing. Firstly, the interference pattern in frequency domain was recorded by optical spectrum analyzer (Yokogawa, AQ6370) with 8.6 THz bandwidth. The measured interference pattern ($i(\nu) = s(\nu) [1 + \cos \phi(\nu)]$) shows sinusoidal modulated shape with period of $1/\tau_{TOF}$ in frequency domain due to optical carrier frequency depended relative phase delay ($\phi(\nu) = 2\pi\nu\tau_{TOF}$). The frequency domain signal is converted into time domain ($I(\tau) = FT\{i(\nu)\} = S(\tau) \otimes [\delta(\tau+\tau_{TOF})/2 + \delta(\tau) + \delta(\tau-\tau_{TOF})/2]$) by Fourier transformation. To simply determine τ_{TOF} , a position of maximum intensity can be chosen, however, its resolution is restricted by temporal resolution of Fourier transformation. It can be enhanced by zero-padding technique, however, it requires much computational time with increasing number of zero-padding points [65,66], and its effect is described in next Section. Alternatively, we have nonlinear curve fitting to finely detect peak position of τ_{TOF} as described in the Methods section of main text. However, such envelope peak detection-based distance metrology cannot support nanometric precision distance measurement. Consequently, to improve measurement precision, we use homodyne detection from microcomb spectral interferometry. A filtered time domain signal near τ_{TOF} is subsequently inverse-Fourier transformed back to the frequency domain as:

$$i'(\nu) = FT^{-1}\{S(\tau) \otimes \delta(\tau-\tau_{TOF})/2\} = [s(\nu)\exp\{i(2\pi\tau_{TOF}\nu)\}]/2 = [s(\nu)\exp\{i\phi(\nu)\}]/2 \quad (1)$$

where $i = (-1)^{1/2}$. This process allows the spectral phase $\phi(\nu)$ to be recovered. The spectral phase can be determined by the formula of $\phi(\nu) = \tan^{-1}[\text{Im}\{s'(\nu)\}/\text{Re}\{s'(\nu)\}]$. Then the target distance can be determined by $L = c/2\nu \times \{M_{\text{Homodyne}} + \phi(\nu)\}$, where M_{Homodyne} is an integer value. Since peak detection-based distance measurement provides accurate distance to be enough to determine integer value M_{Homodyne} , we can use homodyne method with nanometric precision over long range [67, 68].

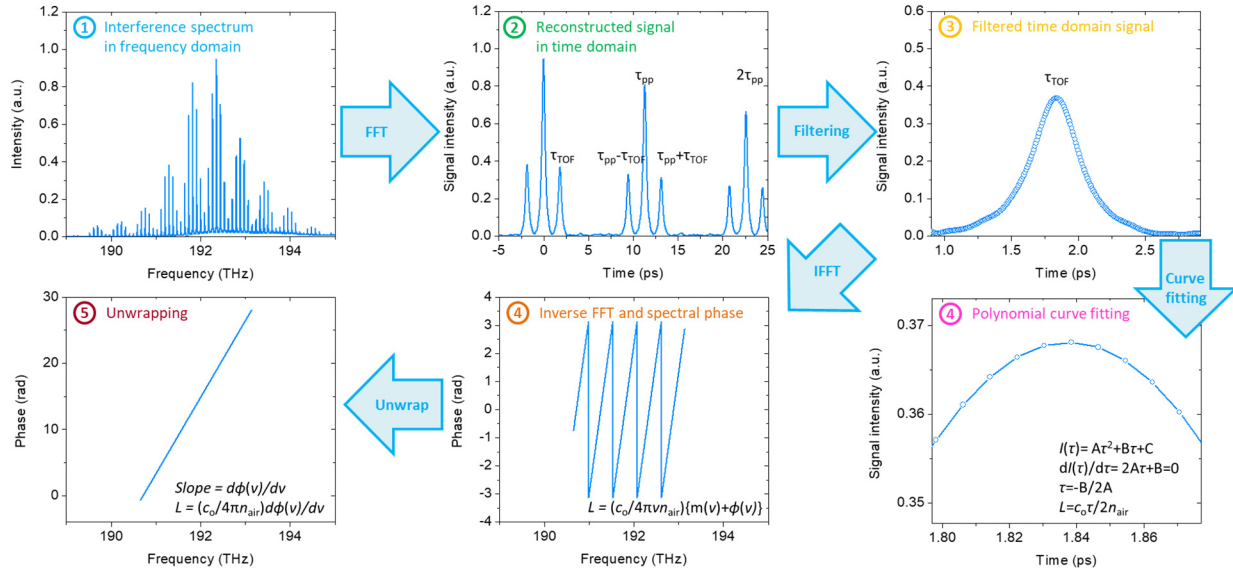


FIG. S1. Data process of spectrally-resolved interferometry. The target distance is determined by two steps. Firstly, time-domain peak detection is used to coarse measurement. Secondly, spectral phase extracted from inverse FFT spectrum from time-domain signal is used to homodyne interferometry for nanometric precision distance measurement. Alternatively, spectral phase slope can be also used to coarse measurement, since the first derivation of the phase delay for optical frequency ν ($d\phi(\nu)/d\nu = 2\pi\tau_{TOF}$) is proportional to τ_{TOF} .

S1.D. Comparison of peak detection method

Zero-padding technique makes Fourier-transformation data to be smoother [69]. If we simply determine τ_{TOF} by reading out the position of maximum intensity, its resolution is limited by 115 fs temporal resolution considering 8.6 THz of spectral range of measured optical spectrum. It means that measured distance is digitized with 115 fs temporal interval as shown in Fig. S2(a). In theory, the temporal resolution of Fourier transformation can be infinitely reduced, however, it comes with a large computational time to achieve high precision distance measurement. However, the measurement precision of nonlinear curve fitting method was found to be near 100 nm whether zero-padding is considered or not. Since the nonlinear curve fitting method do not need to zero-padding for improvement of measurement precision, we determined the distance using this approach. Alternatively, spectral phase slope [70] or cross-correlation methods [71] can be also considered for high-precision peak detection.

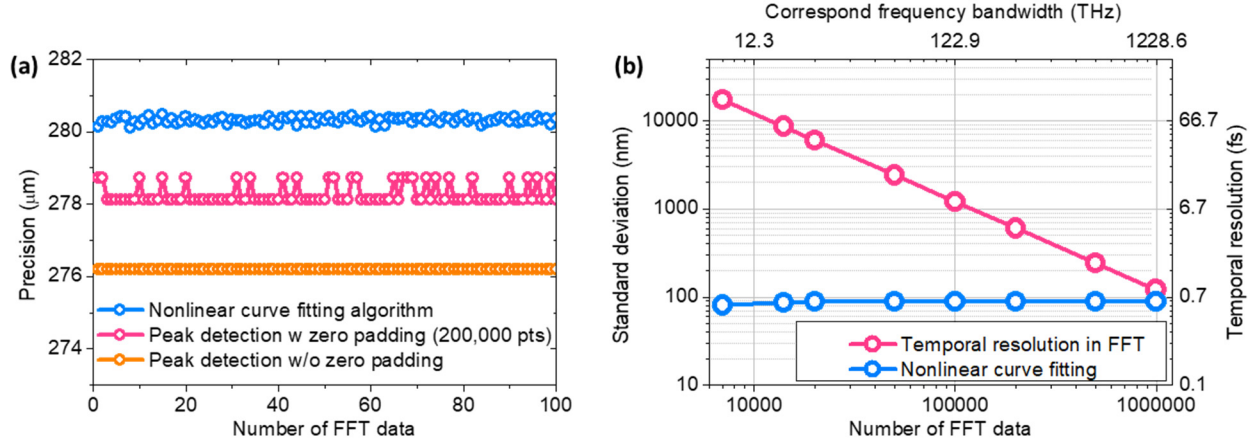


FIG. S2. Precision comparison between peak detection and nonlinear curve fitting method. (a) Time trace of peak detection and nonlinear curve fitting method. For peak detection method, two case (with zero padding and without zero padding) is plotted. For nonlinear curve fitting method, zero padding is not considered. Each result is shifted about 2 μm for comparison. (b) Measurement precision versus number of FFT data for zero padding.

Section S2. Stable dual-pump generation of the single-soliton frequency microcomb

S2.A. Planar-waveguide Si_3N_4 microresonator frequency comb

The microresonator used for the single-soliton frequency comb generation is based on stoichiometric silicon nitride with 261 μm outer radius and 800 nm thickness. The loaded and intrinsic quality factors Q are 1.77×10^6 and 3.4×10^6 respectively. The microresonator width is adiabatically varied from 1 to 4 μm to tune the dispersion and improve the single-mode mode-locking. Using swept-wavelength interferometry, the free spectral range (FSR) is found to be 88 GHz with an anomalous group velocity dispersion β_2 of $-3 \pm 1.1 \text{ fs}^2/\text{mm}$.

S2.B. Counter-propagating dual-pump technique

We set the pump laser (New Focus TLB-6700) at 1595 nm with 23 dBm power and TE polarization. The auxiliary laser (Santec TSL-510) is at 1565 nm with 33 dBm power and TM polarization. The pump laser is set to generate the single-soliton state with counter-clockwise propagation in microresonator. The auxiliary laser wavelength is set for effectively blue-detuning to thermally stabilize the planar waveguide Si_3N_4 microresonator with clockwise propagation, while the pump laser wavelength is set to generate the single-soliton state with counter-clockwise propagation in microresonator. The dual-driven counter-propagating technique separates the thermal hysteresis from the Kerr soliton dynamics [72].

S2.C. Single-soliton generation in microresonator

A single soliton is deterministically generated by cascaded four-wave mixing in the planar waveguide Si_3N_4 microresonator via cross-polarized dual-driven approach. A 33-dBm TM auxiliary laser centered at 1560 nm is sent into the Si_3N_4 microresonator, and slowly detuned into resonance. Then a 24-dBm TE pump is sent into the microresonator in the counter propagation direction [72]. With the thermal hysteresis compensation via the TM auxiliary laser, a single

soliton state is deterministically generated by tuning the TE pump wavelength to the effective red-detuning side of the pump cavity resonance.

Section S3. Repetition rate measurement

To measure the ≈ 88.58 GHz microcomb repetition rate, which is beyond our direct electronic measurement capability, we implemented an electro-optic modulation approach to measure the repetition rate via modulation sidebands. Fig. S3 shows the experimental setup (panel a), measurement approach (panel b), and repetition rate (f_{rep}) measurement for free-running soliton microcomb (panel c). In a nutshell, the microcomb lines separated by 88.5 GHz (f_{rep}) are modulated by an electro-optic phase modulator (EOM), which is driven at 14.355 GHz (f_{EOM}) and generates several orders of optical sidebands between two adjacent comb lines [73]. The EOM-driven sidebands from two adjacent comb lines generate a beat frequency (f_{beat}) at a low-frequency region (≈ 2.45 GHz in our case), which lies within the detection range of our current electronics. The repetition rate (f_{rep}) can thus be determined via the EOM driving frequency and beat frequency with $f_r = n \cdot f_{EOM} + f_{beat}$, where n is the sideband integer number ($n = 3$ in our case) as shown in Fig. S3(b). The beat frequency at low frequency is measured to determine the repetition rate at the high frequency region. In order to characterize the repetition rate stability, the beat frequency f_{beat} is down mixed with another local oscillator (f_{LO}) to tens of MHz level, and then directly measured by frequency counter for over 2,000-sec. The stability results are shown in Fig. S3c. The repetition rate is ≈ 88.5799892 GHz with total drift of 70 MHz over 2,000-sec. The Allan deviation is at the $\approx 7 \times 10^{-8}$ even when up to 400-sec integration time.

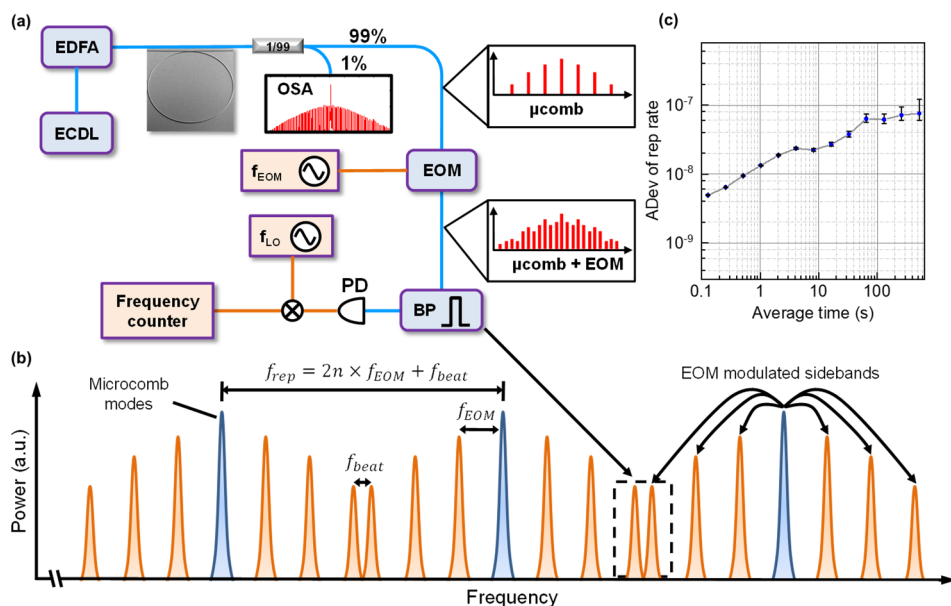


FIG. S3. (a) Measurement configuration for frequency stability of soliton microcomb. (b) Mechanism of repetition rate measurement through EOM modulation. (c) Frequency stability of soliton microcomb in terms of Allan deviation.

Section S4. Position calibration of motorized stage by soliton microcomb-based spectrally-resolved interferometry

To verify the linearity of soliton microcomb based SRI, a motorized stage (New Focus MFN25) is used for comparison measurement. However, its low accuracy for long-stroke translation makes measurement range for the linearity test to be limited less than 150 μm . According to data sheet from manufacturer, on axis accuracy of the motorized stage is 10 μm . To calibrate position error of motorized stage, we compare the stage encoder value and measured distance by fiber comb-based SRI and soliton microcomb based SRI. Our measurement found that on-axis accuracy of the motorized stage is about $\pm 6 \mu\text{m}$ with cycle of 500 μm . This sinusoidal shaped cyclic error might be caused by mechanical structure of the motorized stage. We also found that linearity of the motorized stage is well maintained within 1 μm level at short range of 150 μm . Hence we choose this part for linearity evaluation of soliton microcomb based distance measurement.

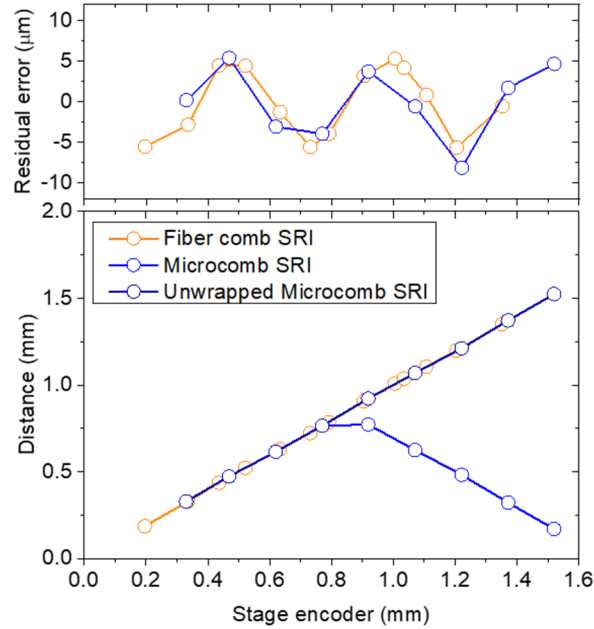


FIG. S4. Evaluating the accuracy of motorized stage by fiber comb and soliton microcomb based. Lower panel shows distance measurement results from fiber comb and microcomb based spectral resolved interferometry versus the motorized stage encoder. Both independent measurements of fiber comb and microcomb based spectral resolved interferometry show positioning error of the motorized stage encoder about $\pm 6 \mu\text{m}$ with cycle of 500 μm .

Section S5. Gauge block measurement for 3D surface

To validate the microcomb SRI for potential 3D surface measurement, we measured a cross-section of a standardized gauge block, used for practical length metrology in 3D surface measurements and industry standards. We replaced the reference mirror in the interferometer part with the gauge block to measure the cross-section of the 3 mm height gauge block (Starrett RCM, 3.0 Al) that has a 300 nm uncertainty. The reference beam is made with a 4% Fresnel reflection

from the end of FC/PC fiber ferrule. The transmitted beam is reflected from the target surface and sent to the optical spectrum analyzer along with the reference beam. The gauge block is mounted on a flat mirror and the stage made an on-axis translation with 1.27 mm (0.05 inch) steps as shown in Fig. S5 (a). The distance at each step is recorded with 5 data points. The gauge block height is determined by the difference of the absolute distances between mirror and gauge block surface, with the same empirical air refractive index of 1.000247 as noted above. The measured cross-section of the gauge block is shown in Fig. S5 (b) and (c). The height of gauge block was found to be 3.001237 mm and 3.001104 mm from the microcomb SRI and homodyne interferometry respectively. We also found a different slope height between the mirror ($1.413\mu\text{m}/\text{mm}$) and gauge block surface ($-1.817\mu\text{m}/\text{mm}$). A tilting (cosine) error from imperfect plane-to-plane alignment may introduce the measurement error of $1.237\mu\text{m}$. As shown in Fig. S5 (d), the measurement repeatability taken over 5 consecutive measurements is determined to be 327 nm and 11.4 nm from microcomb spectral resolved interferometer and homodyne interferometry, respectively as the 1σ standard deviation.

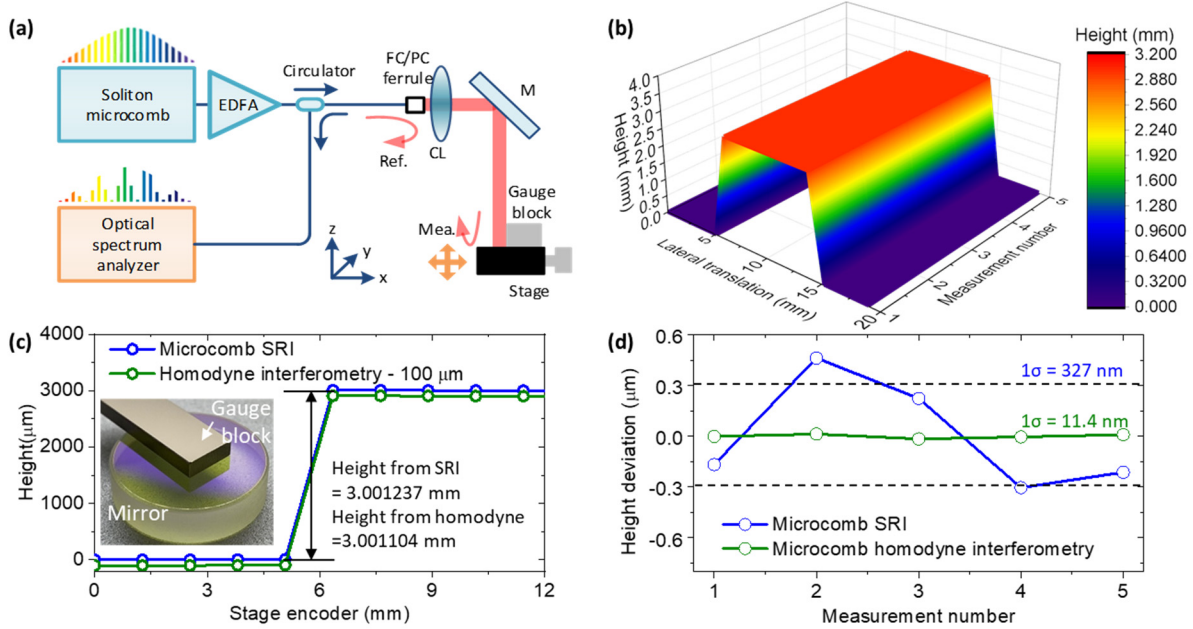


FIG. S5. Measurement of a reference gauge block cross-section via x -axis scanning. Metrology of a reference gauge block cross-section via x -axis scanning. (a) Measurement scheme for cross-section of gauge block with x -axis scanning stage. (b) Reconstructed cross-section of a gauge block. (c) The gauge block height is found to be 3.001237 mm and 3.001104 mm from soliton microcomb spectral interferometry and homodyne interferometry, matching well with reference specified height. (d) Measurement repeatability of the gauge block height.

Section S6. Bounds on the measurement precision of homodyne interferometry.

We found our measurement repeatability of the homodyne interferometry seems to be limited by environmental long-term drift including drift of refractive index of air and thermal expansion of the target distance. To evaluate ultimate measurement precision regardless of the long-term drift, we use 0.05 Hz high pass filter to minimize long-term drift effects on the precision. Fig. S8

shows comparison between raw data and high pass filtered data. For the high pass filtered case, a standard deviation (1σ) is improved to 3.9 nm and slowly-varying fluctuation disappears. If we assume that target is ideally fixed without long-term drift, measurement stability can be improved to be 0.15 nm at 100 seconds averaging time. Such measurement stability is close to commercial HeNe laser interferometry [74].

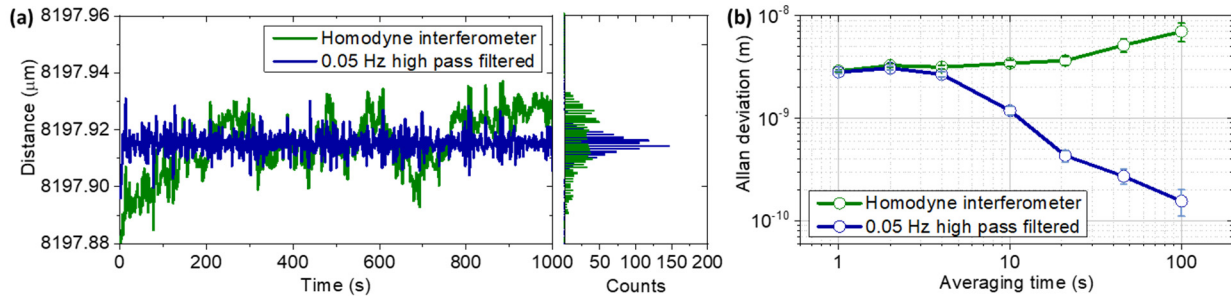


FIG. S6. Evaluation of measurement repeatability of homodyne interferometry. (a) Time trace of homodyne interferometry during 1,000 seconds with raw data marked in yellow color. Its 0.05 Hz high pass filtered data is also plotted with gray color. Right inset shows those histogram (b) Measurement precision in terms of Allan deviation, with 0.05 Hz high pass filtering to remove the long-term drift. Sub-nm measurement stability at 100 seconds averaging can be observed.

Section S7. Reference against a stabilized mode-locked fiber laser frequency comb

A 250 MHz fiber comb (Menlo Systems) stabilized to 1 Hz laser with 10^{-15} fractional frequency stability (Stable Laser Systems) is used to verify our spectrally-resolved interferometry for laser ranging metrology [75, 76]. The fiber comb has optical power of 10 mW and 1560 nm central wavelength. Since the spectrometer cannot resolve the interference pattern when its period is smaller than the resolution of the spectrometer, the measurement range of the fiber comb-based SRI is limited by the resolution of the spectrometer [77]. For this reason, the target distance is fixed near 6 mm. The same interferometer and data processing are used for fiber comb-based SRI. Fig. S7 shows the measurement results of fiber comb-based spectral resolved interferometer. During the measurement of 100 seconds, the measured distance was nearly constant without any notable drift. The measurement repeatability is found to be 85.5 nm (24.5 nm) at averaging time of 1 second (10 seconds). The measurement repeatability of fiber comb-based SRI and soliton microcomb based SRI is almost identical. It means that the noise of soliton microcomb in our approach does not significantly contribute to the measurement repeatability.

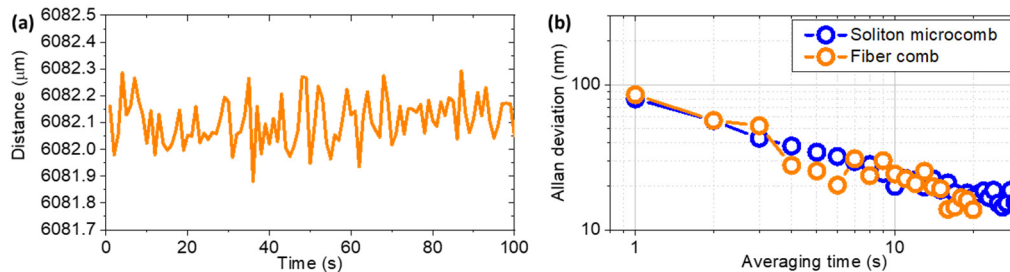


FIG. S7. Measurement result of fiber comb-based SRI. (a) Time trace of fiber comb-based SRI during 100 seconds. (b) Measurement precision in terms of Allan deviation.

Section S8. Characterization of intensity fluctuations on the distance metrology

Intensity fluctuations during the measurement deteriorates the interference pattern in frequency domain, which worsens the measurement precision. To verify this influence, we measure the distance with low and high intensity fluctuation state of soliton microcomb and have numerical simulation. From the interference pattern recorded by optical spectrum analyzer, one of comb line is used to monitor the intensity fluctuation. We investigate for two cases and the measurement results plotted with orange circle. For 3% intensity fluctuation, the standard deviation value of measured distance is found to be 81.6 nm as shown in Figure S6. On the other hand, the standard deviation of measured distance is found to be 469 nm when intensity fluctuation is about 36%. To simulate this situation, one of interference pattern in frequency domain is used and its intensity is modulated by random fluctuation with range of 1% to 50%. Numerical simulation results are plotted in green color and it is quite well-matched with the experimental data. Note that the intensity fluctuations could be generated from the optical spectrum analyzer, the light source itself, polarization variation in the long fiber delay line, and also actual distance variations during measurement.

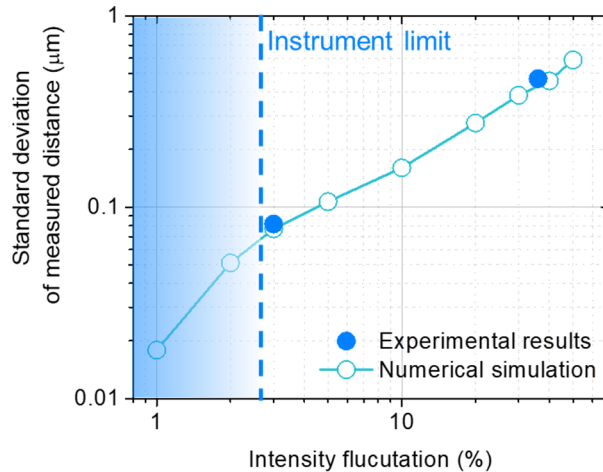


FIG. S8. Intensity fluctuations effects on the measurement precision. Green color denotes numerical simulation results of intensity fluctuation induced measurement precision variation. Blue dot denotes two examples of the experimental results.

In the main text, we demonstrated the spectrally-resolved interferometry provides 3-nm precision with 23-mm non-ambiguity range in the free-running soliton frequency microcomb. With the proportional scaling to longer distances, the measurement precision will depend on the measurement range. In external field-operating scenarios, air refractive index has an $\approx 10^{-6}$ level fluctuation in uncontrolled environments and can be compensated to the 10^{-8} level with well-defined empirical estimates [78] or two-color interferometry [79]. If we assume the air refractive index and target vibrations are negligible, the measurement range dependent imprecision (ΔL) can thus be estimated by $\Delta L = [(3 \text{ nm})^2 + \{(\Delta f/f) \times L\}^2]^{1/2}$. Our spectrally-resolved interferometry approach with both the soliton and comb-line homodyne interferometry can support distance

measurements up to a kilometer or more, since the maximum measurable range (L_{\max}) is bounded by the comb coherence length.

Fig. S9 summarizes our combined metrology specifications and measurement repeatability, scaling as a function of measurement range. Table. S1 and S2 summarizes comparison with other state-of-the-art distance measurement with fiber frequency comb and microcomb, respectively.

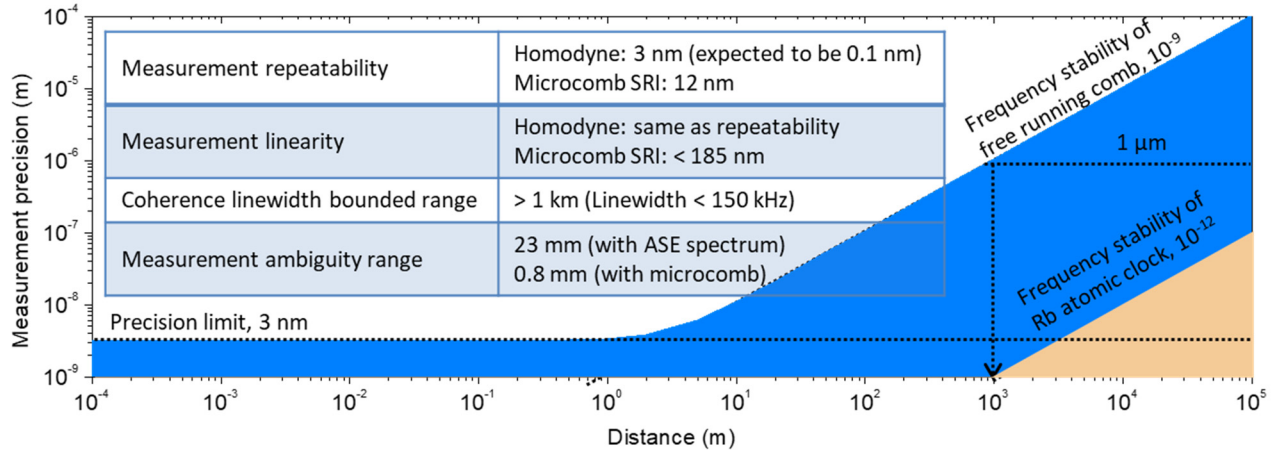


FIG. S9. Metrology specifications and measurement repeatability scaling as a function of measurement range.

Table S1. Summary comparison between fiber/solid-state and our chip-scale distance metrology approaches. Nomenclature: Mod. (modulation); ToF (time-of-flight); SHG (second harmonic generation); CEO (carrier envelope offset); FP (Fabry-Pérot); ASE (amplified spontaneous emission). The bracketed () numbers on the last row shows the measurement precision bounds when environmental air refractive index drift and target thermal expansion are minimized through 0.05 Hz high pass filtering of the interferogram time traces.

Ref.	Metrology approach	Comb/Mod. rep. rate (MHz)	Non-ambiguity range	Linearity error or accuracy (1σ)	Precision (1σ)	Comments
[7]	HeNe laser with dual intensity modulators	28,000	5.5 mm	$\pm 1.1 \mu\text{m}$	undefined	$2f$ mod. and heterodyne
[8]	Dual-fiber laser frequency combs	100.021 & 100.016	1.5 m	homodyne: $\pm 30 \text{ nm}$	5 nm	optical carrier phase
[9]	Fiber femtosecond phase-locked cross-correlation ToF	≈ 100	(large)	undefined	7 nm	Rb-clock locked, SHG
[18]	Fiber mode-locked laser: synthetic wavelength	1,000	1.5 m	$\pm 7 \mu\text{m}$	$7 \mu\text{m}$	20^{th} mode harmonic
[21]	Ti:Sa oscillator: parallel spectral interferometry	1,000	150 mm	homodyne: $\pm 28 \text{ nm}$	undefined	virtual-imaged phase array
[25]	Fiber comb multi-wavelength interferometry	≈ 100	292 mm	$\pm 10 \text{ nm}$	0.5 nm	Rb- and CEO-locked
This work	Chip-scale hybrid single-comb spectral and homodyne interferometry	88,500	23 mm	peak detection: $\pm 185 \text{ nm}$ (homodyne: $\pm 3 \text{ nm}$)	3 nm ($\approx 0.15 \text{ nm}$)	ASE range extension; τ_{avg} at 100 sec.

Table S2. Summary comparison between chip-scale distance metrology approaches. Nomenclature: τ_{ave} (averaging time).

Ref.	Metrology approach	Comb/Mod. rep. rate (MHz)	Non-ambiguity range	Linearity error or accuracy (1σ)	Precision (1σ)	Comments
[42]	Chip-scale dual-comb interferometry	9,360	16 mm	undefined	200 nm	$\tau_{\text{avg}} \approx 0.5$ sec
[43]	Chip-scale dual-comb interferometry	95,842 & 95,746	1.56 mm	± 188 nm	12 nm	$\tau_{\text{avg}} \approx 13$ μ sec
This work	Chip-scale hybrid single-comb spectral and homodyne interferometry	88,500	23 mm	peak detection: ± 185 nm (homodyne: ± 3 nm)	3 nm (≈ 0.15 nm)	ASE range extension; τ_{avg} at 100 sec.

Table S3. Summary comparison of repetition rate stability of free-running comb among different platforms.

Ref.	platform	Repetition rate	Allan deviation @ 100 s	Allan deviation @ 400 s
[48]	Si ₃ N ₄ microring	18 GHz	6×10^{-8}	---
[49]	Silica toroid	86 GHz	6×10^{-7}	---
[16]	Ti: sapphire	50 MHz	2×10^{-8}	8×10^{-8}
[80]	Fiber comb	77 MHz	1×10^{-8}	1×10^{-8}
This work	Si ₃ N ₄ microring	88 GHz	6×10^{-8}	7×10^{-8}

Supplementary References

- [58] K. E. Webb, J. K. Kang, J. Anthony, S. Coen, M. Erkintalo, and S. G. Murdoch, Measurement of microresonator frequency comb coherence by spectral interferometry, *Opt. Lett.* **41**, 277 (2016).
- [59] T. Kippenberg, R. Holzwarth, and S. Diddams, Microresonator-based optical frequency combs, *Science* **332**, 555–559 (2011).
- [60] V. Brasch, M. Geiselmann, T. Herr, G. Lihachev, M. Pfeiffer, M. Gorodetsky, and T. Kippenberg, Photonic chip-based optical frequency comb using soliton Cherenkov radiation, *Science* **351**, 357 (2016).
- [61] D. Cole, E. Lamb, P. DelHaye, S. A. Diddams, and S. Papp, Soliton crystals in Kerr resonators, *Nat. Photon.* **11**, 671 (2017).
- [62] Q. F. Yang, X. Yi, K. Y. Yang, and K. Vahala, Stokes solitons in optical microcavities, *Nat. Phys.* **13**, 53 (2016).
- [63] J. Jin, Y.-J. Kim, Y. Kim, S.-W. Kim, and C.-S. Kang, Absolute length calibration of gauge blocks using optical comb of a femtosecond pulse laser, *Opt. Express* **14**, 5968 (2006).
- [64] G. Wu, L. Liao, S. Xiong, G. Li, Z. Cai, and Z. Zhu, Synthetic wavelength interferometry of an optical frequency comb for absolute distance measurement, *Sci. Rep.* **8**, 4362 (2018).

- [65] K. G. Larkin, Efficient nonlinear algorithm for envelope detection in white light interferometry, *J. Opt. Soc. Am. A* **13**, 832 (1996).
- [66] C. Dorrer, N. Belabas, J.-P. Likforman, and M. Joffre, Spectral resolution and sampling issues in Fourier-transform spectral interferometry, *J. Opt. Soc. Am. B* **17**, 1795 (2000).
- [67] S. A. van den Berg, S. van Eldik, and N. Bhattacharya, Mode-resolved frequency comb interferometry for high-accuracy long distance measurement, *Sci. Rep.* **5**, 14661 (2015).
- [68] B. K. Kim and K.-N. Joo, A multi-channel fiber optic proximity sensor, *Meas. Sci. Technol.* **27**, 035104 (2016).
- [69] J. Park, J. Jin, J.-A. Kim, and J. W. Kim, Absolute distance measurement method without a non-measurable range and directional ambiguity based on the spectral-domain interferometer using the optical comb of the femtosecond pulse laser, *App. Phys. Lett.* **109**, 244103 (2016).
- [70] K.-N. Joo, Y. Kim, and S.-W. Kim, Distance measurements by combined method based on a femtosecond pulse laser, *Opt. Express* **16**, 19799-19806 (2008).
- [71] S. Han, Y.-J. Kim, and S.-W. Kim, Parallel determination of absolute distances to multiple targets by time-of-flight measurement using femtosecond light pulses, *Opt. Express* **23**, 25874-25882 (2015).
- [72] H. Zhou, Y. Geng, W. Cui, S.-W. Huang, Q. Zhou, K. Qiu, and C. W. Wong, Soliton bursts and deterministic dissipative Kerr soliton generation in auxiliary-assisted microcavities, *Light: Sci. & Appl.* **8**, 50 (2019).
- [73] P. Del’Haye, S. B. Papp, and S. A. Diddams, Hybrid electro-optically modulated microcombs, *Phys. Rev. Lett.* **109**, 263901 (2012).
- [74] D. Voigt, J. D. Ellis, A. L. Verlaan, R. H. Bergmans, J. W. Spronck, and R. H. Munnig Schmidt, Toward interferometry for dimensional drift measurements with nanometer uncertainty, *Meas. Sci. Technol.* **22**, 094029 (2011).
- [75] R. J. Jones, I. Thomann, and J. Ye, Precision stabilization of femtosecond lasers to high-finesse optical cavities, *Phys. Rev. A* **69**, 051803 (2004).
- [76] T. M. Fortier, M. S. Kirchner, F. Quinlan, J. Taylor, J. C. Bergquist, T. Rosenband, N. Lemke, A. Ludlow, Y. Jiang, C. W. Oates, and S. A. Diddams, Generation of ultrastable microwaves via optical frequency division, *Nat. Photon.* **5**, 425 (2011).
- [77] G. Tang, X. Qu, F. Zhang, X. Zhao, and B. Peng, Absolute distance measurement based on spectral interferometry using femtosecond optical frequency comb, *Opt. Lasers Eng.* **120**, 71-78 (2019).
- [78] P. E. Ciddor, Refractive index of air: new equations for the visible and near infrared, *Appl. Opt.* **35**, 1566–1573 (1996).
- [79] G. Wu, M. Takahashi, K. Arai, H. Inaba, and K. Minoshima, Extremely high-accuracy correction of air refractive index using two-colour optical frequency combs, *Sci. Rep.* **3**, 1894 (2013).
- [80] K. Jung and J. Kim, Characterization of timing jitter spectra in free-running mode-locked lasers with 340 dB dynamic range over 10 decades of Fourier frequency, *Opt. Lett.* **40**, 316 (2015).